Effect of Sn dopant on the properties of ZnO nanowires

2004 J. Phys. D: Appl. Phys. 37 2274

(http://iopscience.iop.org/0022-3727/37/16/009)

INSTITUTE OF PHYSICS PUBLISHING JOURNAL OF PHYSICS D: APPLIED PHYSICS

J. Phys. D: Appl. Phys. **37** (2004) 2274–2282 PII: S0022-3727(04)78783-5

Effect of Sn dopant on the properties of ZnO nanowires

Seu Yi Li[1], Pang Lin[1], Chia Ying Lee[2], Tseung Yuen Tseng[2,4] and Chorng Jye Huang[3]

[1] Institute and Department of Materials Science and Engineering, National Chiao Tung University, Hsinchu, 300, Taiwan, Republic of China
[2] Department of Electronics Engineering and Institute of Electronics, National Chiao Tung University, Hsinchu, 300, Taiwan, Republic of China
[3] Materials Research Laboratories, Industrial Technology Research Institute, Hsinchu, 310, Taiwan, Republic of China

E-mail: tseng@cc.nctu.edu.tw

Received 6 April 2004
Published 28 July 2004
Online at stacks.iop.org/JPhysD/37/2274
doi:10.1088/0022-3727/37/16/009

Abstract
Sn doped ZnO (SZO) nanowires were fabricated by a vapour–liquid–solid growth process. The reaction temperature for the formation of the nanowires can be reduced to ∼100°C due to Sn doping. The growth direction and morphology of SZO nanowires depend on the amount of Sn, which is attributed to the difference in sizes between Zn and Sn atoms. The ultraviolet emission of SZO nanowires varies from 380 to 396 nm since Sn acts as a doubly ionized donor and introduces deep states in the band gap. In addition, the SZO nanowires exhibit significantly improved field emission characteristics with a turn-on electric field of 0.05 V μm^{-1} under a current density of 0.5 mA cm^{-2} in comparison with undoped ZnO nanowires. The work function of the SZO nanowire decreases for higher carrier concentrations and the field enhancement factor increases for smaller diameters. Also, the resistance of the SZO nanowire is decreased for the higher Sn mole fraction. Therefore, it is expected that SZO nanowires can be applied in nano-lasers and flat panel displays in the future.

1. Introduction

ZnO, a direct band gap (3.37 eV) semiconductor with exciton binding energy of 60 meV, is a suitable material for optical application. Much attention has been directed towards the understanding of the growth mechanisms, physical properties, optical characteristics and field emission applications [4–8] of interesting ZnO nano-structures, such as nanowires [1], nanobelts [2], and nanoneedles [3]. Recently, it has been reported that the larger aspect ratio of the ZnO nanowires used in field emission studies can provide lower threshold power density [9–12]. The vapour–liquid–solid (VLS) process [13–15] has the advantages of high aspect ratio, geometric control, low production cost, and large area deposition over other growth methods like metal–organic vapour phase epitaxy deposition (MOVPE) [16], template method [17], hydrothermal method [18], etc. Therefore, it is suitable for growing ZnO nanowires with good field emission characteristics and is used to synthesize the nanowires in this study.

It is well known that the structural properties and dopants may determine the electronic and photoluminescence (PL) properties of the material. The typical dopants that have been used to enhance the conductivities of ZnO are the group III (B, Al, In, Ga) and group IV (Pb, Sn) elements of the periodic table. Sn can serve as a doubly ionized donor with the incorporation of SnO_2 as a solute in ZnO and, consequently, provide high electron carrier concentration. It is, therefore, expected that the Sn doped ZnO (SZO) nanowires have higher electrical conductivity and better field emission properties compared to undoped ZnO nanowires.

In this work, the effects of varying the concentration of Sn as a dopant on the surface morphology, crystal structure,

[4] Author to whom any correspondence should be addressed.

chemical composition, PL, and field emission characteristics of the undoped and SZO nanowires were investigated.

2. Experiment

To prepare the p-type Si(100) substrate for the synthesis of SZO nanowires, the substrate was cleaned by the standard Radio Corporation of America (RCA) cleaning method. After cleaning, rf-sputtering (13.56 MHz) was adopted to deposit an ultra-thin Au catalyst film (∼60 Å thick) under Ar sputtering gas (5.0 cm^3 min^{-1}) at 20 mTorr for ∼10–30 s. Our synthesis process was performed by a VLS fabrication process. The ball-milled (24 h) and mixed powders of ZnO, SnO_2, and carbon (Alfa Aesar, 99.995%) consisted of 0, 0.1, and 0.3 mole fractions of Sn. Then, the mixed powder was loaded into a quartz boat and placed in the centre of a quartz tube. The cleaned p-Si(100) substrate was loaded into the lower temperature region of the quartz boat. The quartz tube was laid in a horizontal furnace. The synthesis temperature of the VLS process of undoped ZnO and SZO nanowires were ∼900°C and ∼800°C, respectively. High purity Ar gas was used as carrier gas with a gas flow rate of 50–100 cm^3 min^{-1}.

The crystal structure of the SZO nanowires was studied by x-ray diffraction (XRD, MAC Science, MXP18, Japan). The microstructures of the undoped and SZO nanowires were analysed by field emission scanning electron microscopy (FE-SEM, Hitachi S-4700I, Japan) and high resolution transmission electron microscopy (HR-TEM, Philips tecani-20, USA). The chemical composition of the SZO nanowires was characterized by analytical transmission electron microscopy (AEM/EDS, JEOL JEM-2010, Japan). The composition and chemical bonding of the SZO nanowires were analysed by x-ray photoelectron spectroscopy (XPS VG Scientific ESCALAB 250, UK) and Auger electron microprobe spectroscopy (AES VG Scientific ESCALAB 350, UK), respectively. A PL analyser (Hitachi F-4500, Japan) with a Xe lamp as an excitation source (325 nm) was used for optical emission studies at room temperature.

The field emission characteristics were measured by the Keithley 237 current–voltage (I–V) analyser, which provided the sweeping electric field and monitored the emission current at a base pressure of 1×10^{-8} Torr at room temperature. The distance between the upper tungsten electrode probe and the SZO nanowires was 300 μm, which was adjusted by a precision screw-meter with an accuracy of ± 1 μm and the area of this electrode was 0.028 cm^2.

3. Results and discussion

The ZnO nanowires were grown in a horizontal quartz tube furnace. The p-Si(100) substrate and ZnO, SnO_2, and carbon ball mixed powders were loaded into the quartz tube. The p-Si(100) substrate was put in the lower temperature zone of the furnace. In each experiment, those substrates were loaded in the same position. During the synthesizing process, high purity Ar gas as an auxiliary gas was introduced into the fabrication system with a flow rate of 50–100 cm^3 min^{-1}. The growth process continued at 800–900°C for 12–20 min.

Figure 1(a)–(c) indicate the XRD patterns of the ZnO nanowires with 0, 0.1, and 0.3 mole fractions of Sn, respectively. The pure ZnO nanowires synthesized at 900°C (figure 1(a)) are of hexagonal structure as reported in the Joint Committee on Powder Diffraction Standards–International Centre for Diffraction Data (JCPDS–ICDD)[19] no. 80-0074. The reaction temperature for the formation of the SZO nanowires is not so high as that of the undoped ZnO nanowires. It is suggested that SnO_2 reacts with carbon to form Sn vapour according to the following chemical reaction:

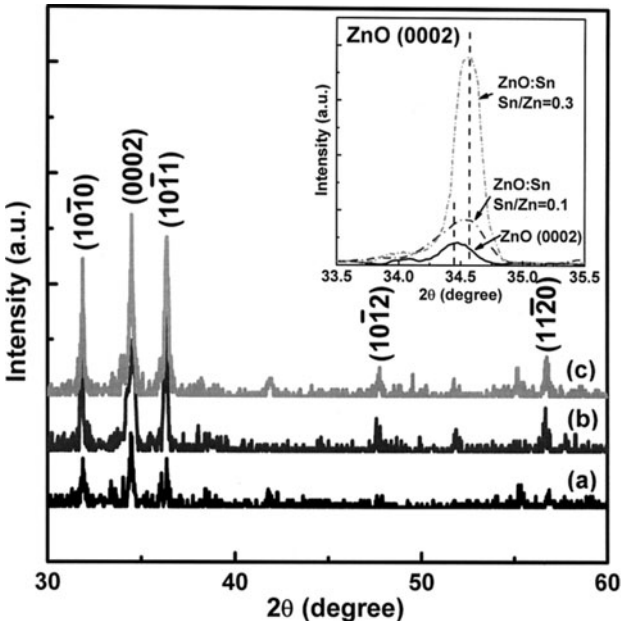

Figure 1. XRD patterns of the (a) ZnO, (b) 0.1, and (c) 0.3 SZO nanowires. The inset is (0002) peak shifted by Sn dopant.

$$SnO_{2(s)} + 2C_{(s)} \rightarrow Sn_{(g)} + 2CO_{(g)}. \quad (1)$$

The generated Sn vapour would initiate a catalyst droplet-assisted growth in the early stage of the VLS process. While we mixed SnO_2 and ZnO source powders with carbon, the synthesized temperature can be decreased to ∼800°C.

The SZO nanowires synthesized at 800°C with 0.1 (figure 1(b)) and 0.3 (figure 1(c)) mole fractions of Sn have similar characteristic peaks as the pattern shown in figure 1(a), but the angle 2θ of the (0002) peak has a small shift from 34.40° to 34.52°. The SZO nanowires still have a hexagonal structure and possess shorter lattice parameters compared to the undoped ZnO nanowires. The lattice constants of the undoped ZnO nanowires are $a = b = \sim 3.52$ Å and $c = \sim 5.21$ Å, those of the 0.1 SZO nanowires are $a = b = \sim 3.49$ Å and $c = \sim 5.19$ Å, and those of the 0.3 SZO nanowires are $a = b = \sim 3.43$ Å and $c = \sim 5.18$ Å, which can be calculated according to the XRD patterns. If the addition of SnO_2 to ZnO forms a substitutional solid solution with the hexagonal structure, a possible reaction is

$$SnO_{2(s)} \xrightarrow{ZnO} Sn_{Zn}^{\bullet\bullet} + 2O_O + V_{Zn}'', \quad (2)$$

where $Sn_{Zn}^{\bullet\bullet}$ means Sn substituted for Zn^{2+} in ZnO, O_O denotes O at the oxygen site, and V_{Zn}'' indicates a vacancy at a Zn^{2+} site in the lattice of the SZO nanowires. It is shown in equation (2) that a Sn^{4+} atom is substituted for a Zn^{2+} atom, and a Zn vacancy

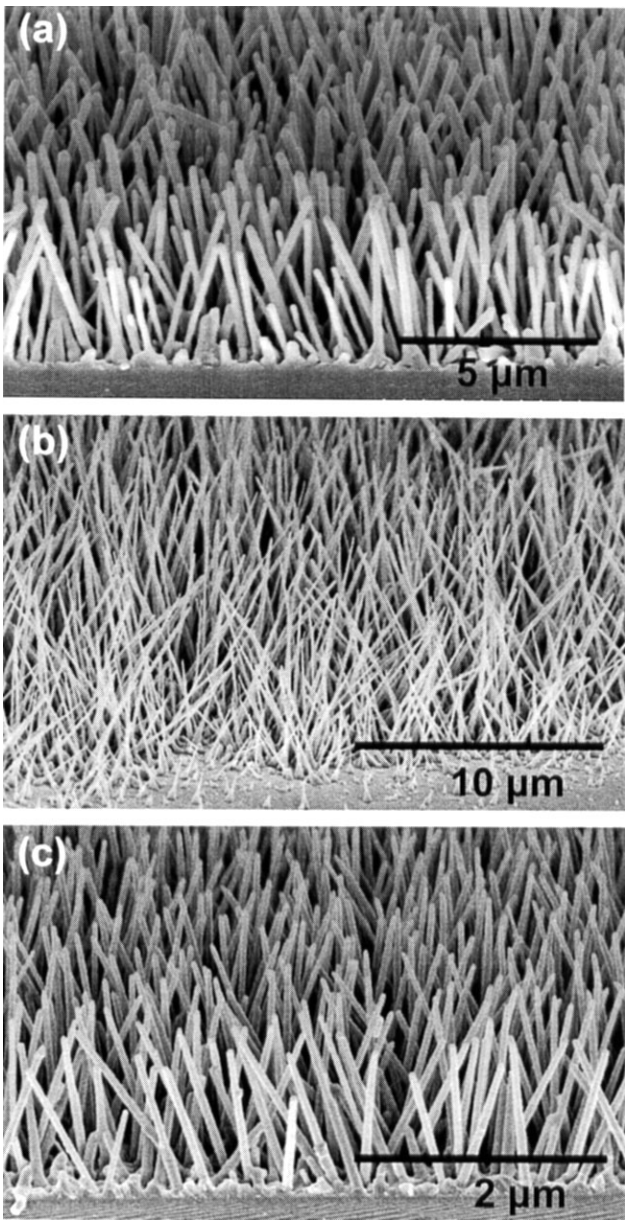

Figure 2. SEM images of the (*a*) ZnO, (*b*) 0.1, and (*c*) 0.3 SZO nanowires.

forms. The shorter lattice constants in the SZO nanowires may be attributed to smaller ionic radii of Sn^{4+} ($r_{Sn}^{4+} = 0.069$ nm, $r_{Zn}^{2+} = 0.074$ nm) and the formation of a Zn vacancy.

The tilted 45°-viewed FE-SEM images of undoped and SZO nanowires on p-Si(100) substrates are demonstrated in figure 2, indicating that the surface morphologies of the nanowires depend strongly on the amount of the dopant, Sn. As shown in figure 2(*a*), the undoped ZnO nanowires have smooth sidewalls, uniform diameter of ∼50 nm, and length of ∼5 μm. Figures 2(*b*) and (*c*) show the geometrical appearances of the 0.1 and 0.3 SZO nanowires, respectively. Under equal thickness of the Au catalyst film (∼60 Å), the dimensions such as length and diameter of the ZnO nanowires should be similar due to the same thermal synthesized process and carrier gas flow rate being used. But a very interesting aspect is the different morphologies for 0.1 and 0.3 SZO

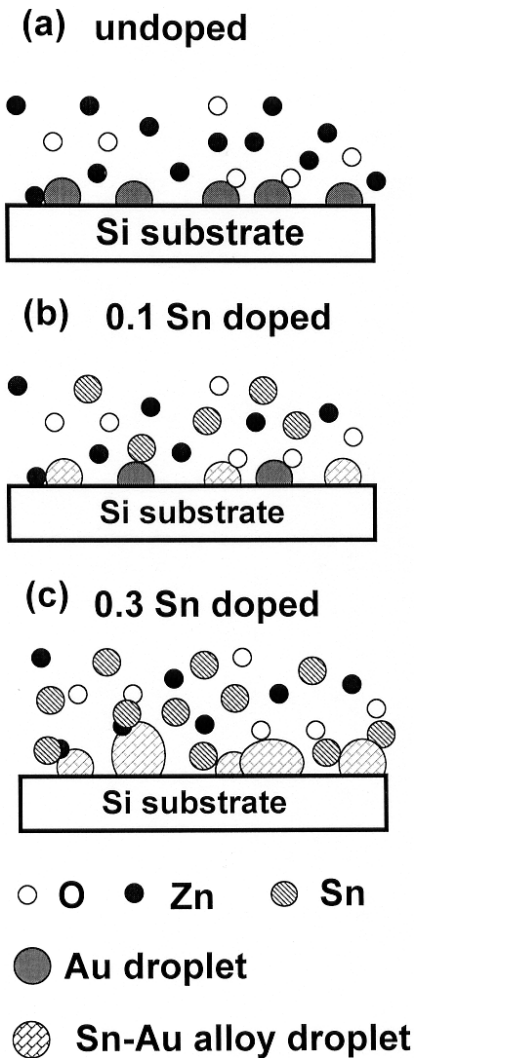

Figure 3. VLS growth process mechanism for, (*a*) undoped, (*b*) 0.1, and (*c*) 0.3 SZO nanowires.

nanowires. These two nanowires have rugged sidewalls, smaller diameters, and longer lengths. The 0.1 SZO nanowires have a diameter of ∼30 nm and length of ∼10 μm, while the 0.3 SZO nanowires have a diameter of ∼80 nm and length of ∼2 μm. The individual average volume of the undoped, 0.1, and 0.3 SZO nanowires are of the same order and comparable. The values are $\sim 9.817 \times 10^{-3}$ μm^3, $\sim 7.068 \times 10^{-3}$ μm^3, and $\sim 10.053 \times 10^{-3}$ μm^3, respectively. According to the alloy phase diagram of Au and Sn, at a temperature of ∼282°C, Au and Sn form a eutectic Au–Sn alloy (20 wt% Sn and 80 wt% Au) [20]. Therefore, the 0.1 SZO nanowires have smaller diameters and larger lengths because of the low partial pressure of Sn in the vapour phase upstream, which leads to the deposition of Sn as small droplets that alloy with Au on the substrate, thus initiating the growth of longer nanowires in the presence of sufficient Zn vapour in the VLS process. In contrast, the 0.3 SZO nanowires have larger diameter and shorter length due to the presence of abundant Sn vapour, which leads to the formation of larger Au–Sn catalyst droplets under a lower Zn vapour pressure. The Sn-assisted growth mechanism of undoped and SZO nanowires is schematically shown in figure 3. The Sn in the alloy droplets can diffuse into

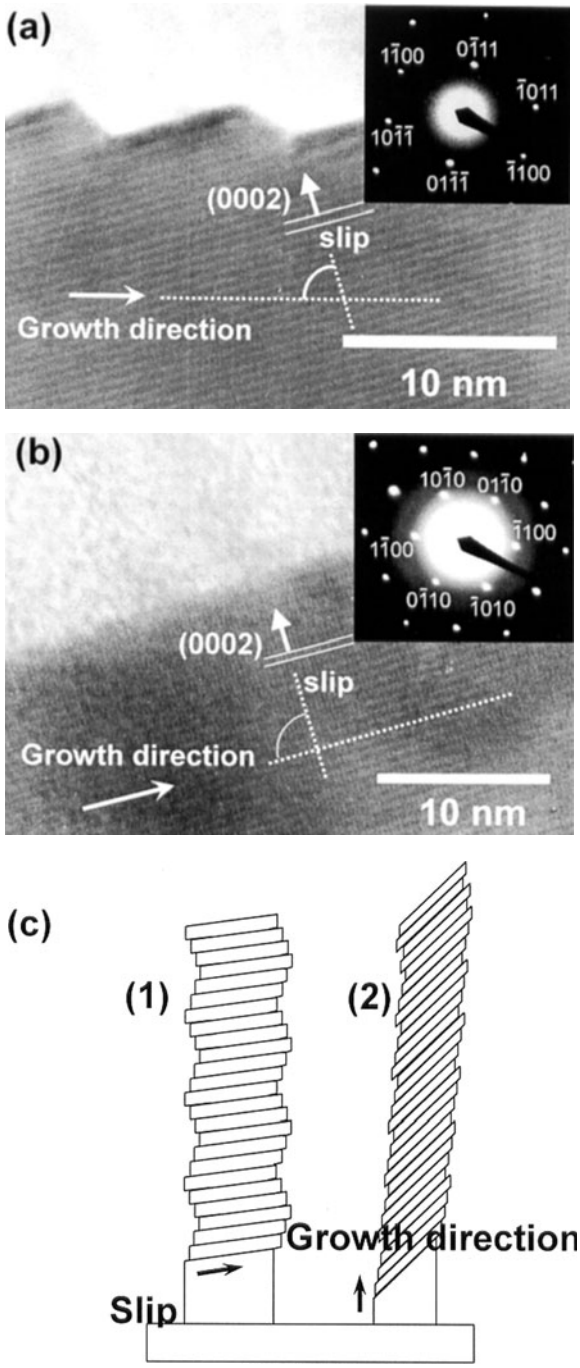

Figure 4. (*a*) HR-TEM images of the 0.1 SZO nanowires. The (0002) lattice fringe is tilted by about 70° with respect to the growth direction. The inset is the SAED pattern. (*b*) HR-TEM images of the 0.3 SZO nanowires. The (0002) lattice fringe is tilted by about 88° with respect to the growth direction. The inset is the SAED pattern. (*c*) The slip structure with the different molar fractions of Sn in SZO nanowires.

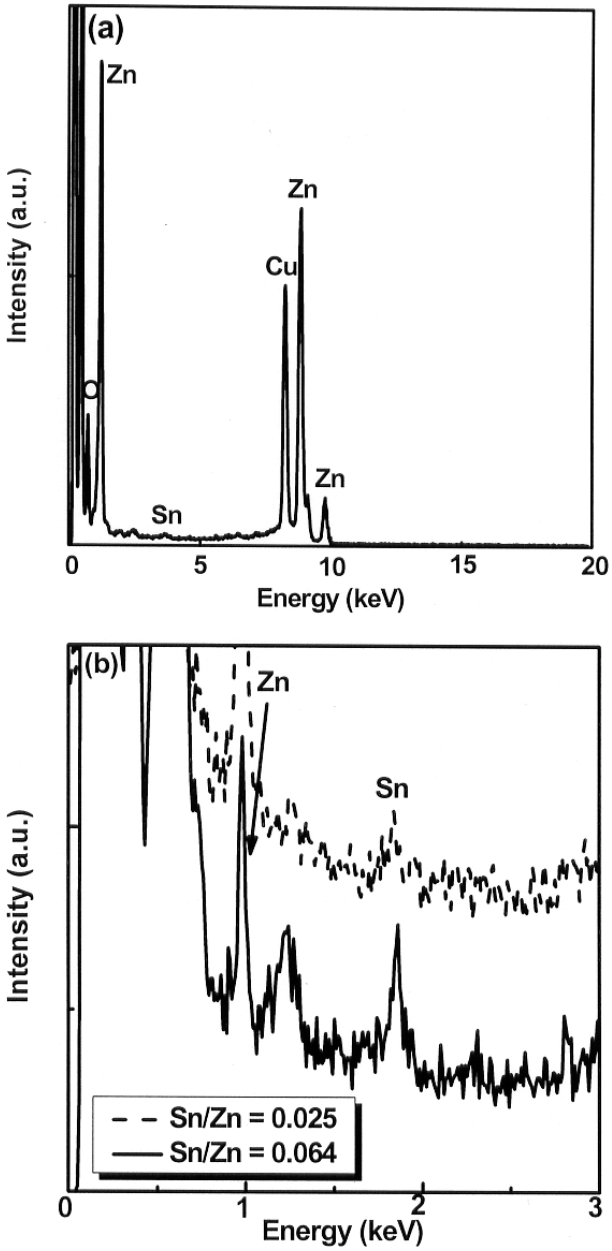

Figure 5. (*a*) EDS spectrum of the SZO nanowires and (*b*) enlarged EDS spectra of the SZO nanowires.

ZnO nanowires through the thermal process. The content of Sn in the SZO nanowires can be measured by EDS spectra, as demonstrated in a later section. This indicates that the fraction of Sn to Zn can influence the morphologies of the SZO nanowires.

The HR-TEM images of the SZO nanowires shown in figure 4 depict the effect of doping on the slip system. The clear lattice fringes of (0002) planes of 0.1 SZO nanowires are indicated in figure 4(*a*) and there is an included angle of ∼70° between the [0002] direction and the growth direction. The distance between each lattice fringe is 3.49 Å, which matches the lattice constants ($a = b = \sim 3.49$ Å and $c = \sim 5.19$ Å) obtained from the XRD analysis (figure 1). The 0.3 SZO has ∼3.43 Å between two (0002) planes (figure 4(*b*)), which is also consistent with XRD results ($a = b = \sim 3.43$ Å and $c = \sim 5.19$ Å.) with an included angle of ∼88° between the [0002] direction and the growth direction. The accurate values of Sn content of 0.1 and 0.3 Sn doped SZO nanowires are ∼0.24 at.% and ∼0.60 at.%, respectively, on the basis of the AEM-EDS and XPS analysis results obtained in the later section. Such an increase in the included angle with an increase in Sn concentration (figure 4) may be attributed to larger compressive

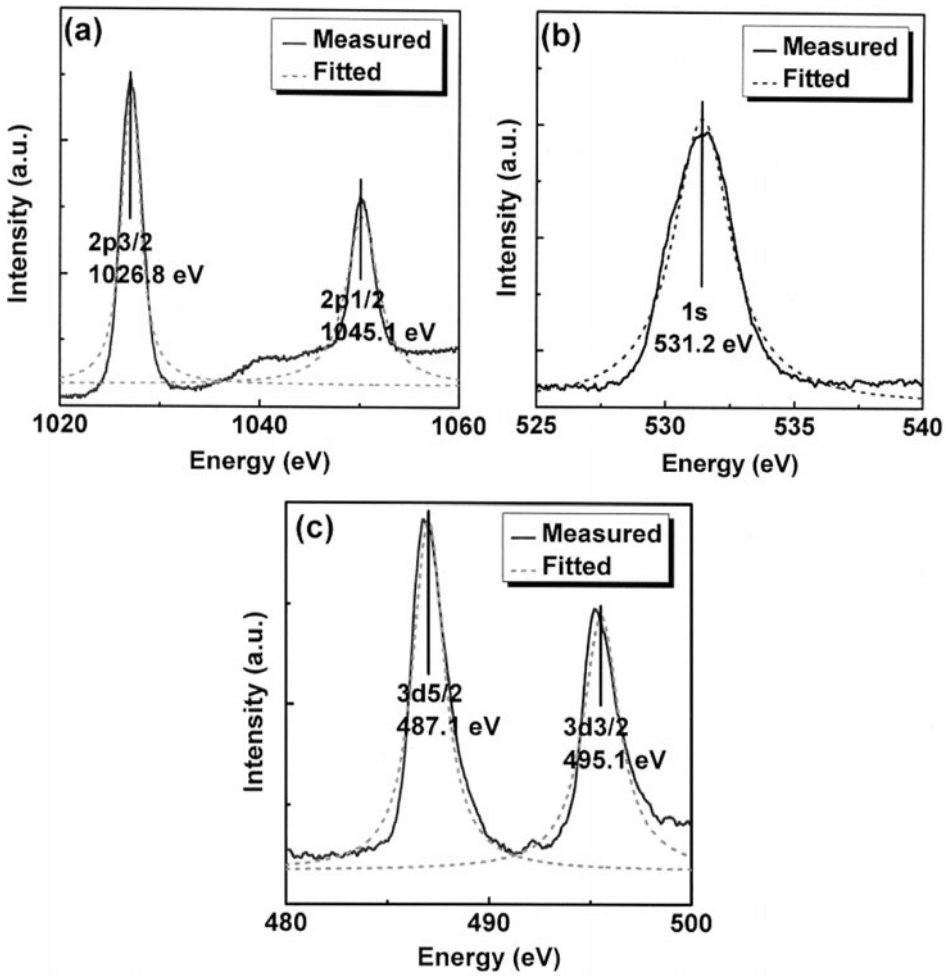

Figure 6. XPS spectra of the 0.3 Sn doped SZO nanowires, (*a*) Zn spectrum, (*b*) O spectrum, and (*c*) Sn spectrum.

stresses generated in higher Sn concentration nanowires, arising from the difference in thermal expansion coefficients as a result of the smaller ionic radii of Sn in comparison with that of Zn ($r_{Zn^{2+}} = 0.074$ nm and $r_{Sn^{4+}} = 0.069$ nm), and the higher number of Zn vacancies existing in higher Sn doped nanowires based on equation (2). That is, the enhanced compressive stress and increased amount of Zn vacancies in higher Sn doped nanowires would consequently lead to a larger included angle between the [0002] direction and the growth direction. Therefore, the variation of mole fraction of the dopant Sn would influence the internal stress resulting in different slip structures of the SZO nanowires (figure 4(*c*)). The SAED patterns shown in the insets of figures 4(*a*) and (*b*) indicate the $[01\bar{1}0]$ direction and hexagonal structure of the SZO nanowires, respectively.

The AEM-EDS spectra of the SZO nanowires are shown in figure 5. Figure 5(*a*) is a typical spectrum of SZO nanowires and the corresponding chemical compositions have also been marked (the Cu peaks come from the Cu TEM grid). It reveals that zinc (Zn), oxygen (O), and tin (Sn) are the constituent parts of the SZO nanowires, and the compositions are uniform along the growth direction. The EDS measurements show that the dominant composition is $Zn_{0.977}Sn_{0.024}O$ for the 0.1 SZO and $Zn_{0.941}Sn_{0.060}O$ for the 0.3 SZO nanowires. The measured Sn at.% may be due to the diffusion of excess Sn from the Sn saturated Au–Sn alloy droplet. At the beginning of the VLS fabrication process, Sn is expected to form a eutectic alloy with Au. Upon extending the fabrication time, the Sn partial pressure gets saturated. This leads to precipitation of Sn from the Au–Sn alloy and its diffusion into the ZnO nanowires. This means, that most of the Sn remain in front of the metal tip of the SZO nanowires and adapt to burning away by a longer synthesized time under flowing carrier Ar gas. Therefore, the Sn doping concentration of the SZO nanowires depends on the SnO_2 mole fraction presented in the ball milled and mixed powders.

The XPS spectra of 0.3 Sn doped nanowires are shown in figure 6, indicating that the Sn^{4+} has substituted for Zn^{2+} and hence a Zn vacancy has formed. In figure 6(*a*), $Zn_{2p3/2}$ and $Zn_{2p1/2}$ peaks are located at 1026.8 eV and 1045.1 eV, respectively, and in figure 6(*b*), the O_{1s} is located at 531.2 eV. Based on the binding energy spectra, the $Zn_{2p3/2}$ and $Zn_{2p1/2}$ peaks that appear, respectively, at 1026.8 eV and 1045.1 eV coincide with the previous XPS findings for ZnO [21]. The O_{1s} peak at 531.2 eV is attributed to oxidized ions in ZnO nanowires. Furthermore, the $Sn_{3d5/2}$ and $Sn_{3d3/2}$ peaks shown in figure 6(*c*) are located at 487.1 eV and 495.1 eV, respectively, which can be attributed to Sn ions in the SZO nanowires. The mole fraction of Zn/Sn/O is ∼0.934/0.067/1.000 calculated from XPS data, which agrees reasonably with the AEM-EDS

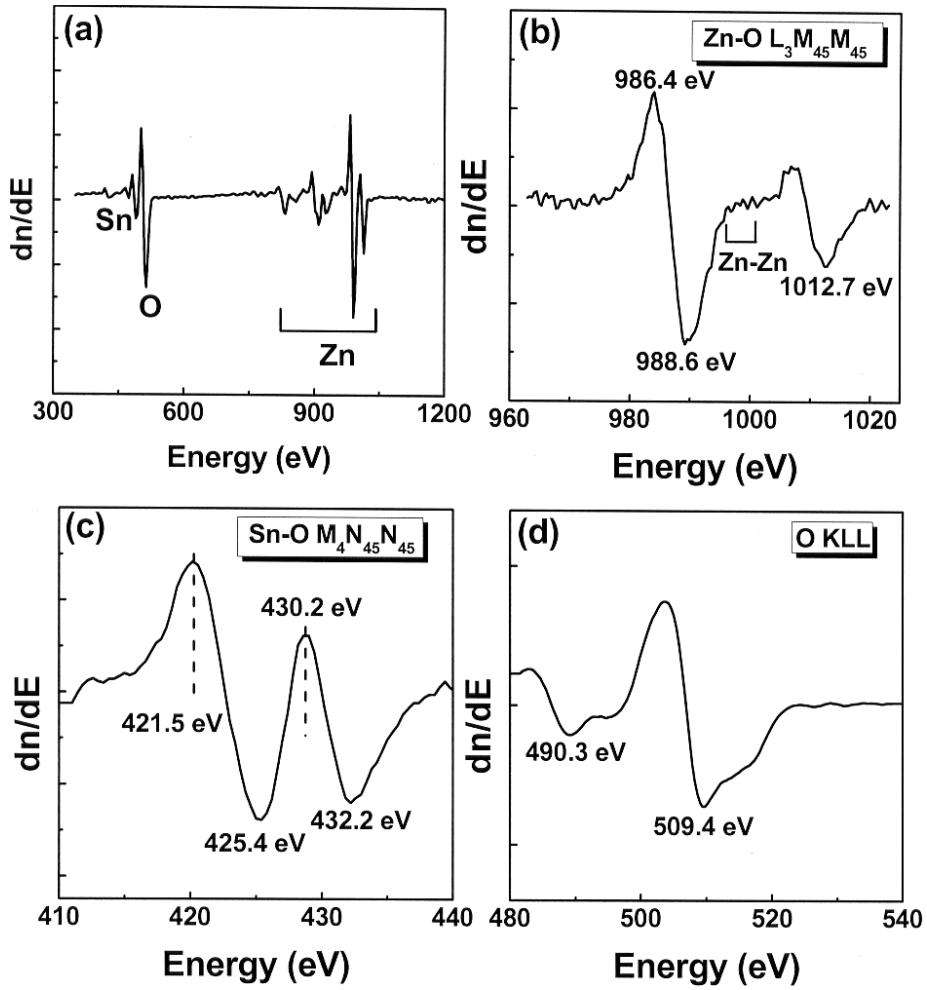

Figure 7. AES differential spectra of the 0.3 Sn doped SZO nanowires, (*a*) full scale scanning results. (*b*) Zn spectrum, (*c*) O spectrum, and (*d*) Sn spectrum.

result for 0.3 Sn doped nanowires. The chemical state energies of the detected Sn and O in the SZO nanowires exhibit Sn–O bond formation, that is, the Sn atom can diffuse into the ZnO nanowires and the Zn^{2+} is substituted by Sn^{4+}, leading to an increase in the concentration of electrons, and this will consequently lead to better field emission characteristics of the SZO nanowires, which is described in a subsequent section.

The high resolution AES chemical composition spectra of 0.3 Sn doped SZO nanowires can further decide the bonding between the atoms of SZO nanowires. Figure 7(*a*) is an AES spectrum of the SZO nanowires scanned in the full scanning range (300–1200 eV). After differential calculation analysis, some obvious peaks indicate that Sn, Zn, and O are located at 400–440 eV, 990–1020 eV, and 480–510 eV, respectively, [21]. The detailed high resolution binding energy spectra of individual elements are shown in figures 7(*b*)–(*d*). The AES spectrum of Zn (figure 7(*b*)) indicates clear peaks at 986.4, 988.6, and 1012.7 eV corresponding to the LMM Auger electron emissions from the Zn–O bonds. The vibration curve between 991.6 and 995.2 eV results from Zn–Zn bonds. Figure 7(*c*) shows the MNN emissions of Sn–O bonds, which are located at 421.5, 430.2, and 432.4 eV while the 425.4 eV emission results from Sn–Sn bonds. Lastly, the oxygen KLL emissions of 490.3 and 509.4 eV are indicated in figure 7(*d*). On the basis of AES results, we may presume that the Sn substitutes Zn and binds with O in the SZO nanowires, which is in agreement with the result of XPS analysis.

Figure 8(*a*) shows the room temperature (298 K) PL spectra of undoped ZnO and SZO nanowires. A strong ultraviolet (UV) emission at 380 nm and a green light emission at 520 nm are observed in the PL spectrum of the undoped ZnO nanowires. The UV emission is due to the direct band gap of ZnO, and the green light emission corresponds to the oxygen vacancies in the ZnO nanowires. On the other hand, it illustrates that the SZO nanowires exhibit four PL bands centred at 380, 396, 461, and 502 nm. Corresponding to the band gap value of the SZO nanowires shown in figure 8(*b*), those two emission peaks at 380 nm ($E_\lambda = 3.26$ eV) and 396 nm ($E_\lambda = 3.13$ eV) could be attributed to (1) the recombination of electrons in the valence band with holes in the conduction band, and (2) the recombination of electrons in deep traps with holes in the conduction band, respectively. These processes are shown in figure 8(*c*). It is suggested that the first peak of 380 nm corresponds to the band gap of ZnO, and the second peak of 396 nm may be due to the response for the Sn atom that performs the role of a doubly ionized donor and introduces deep states in the energy band gap (see figure 8(*c*)). As a result, the peak intensity of

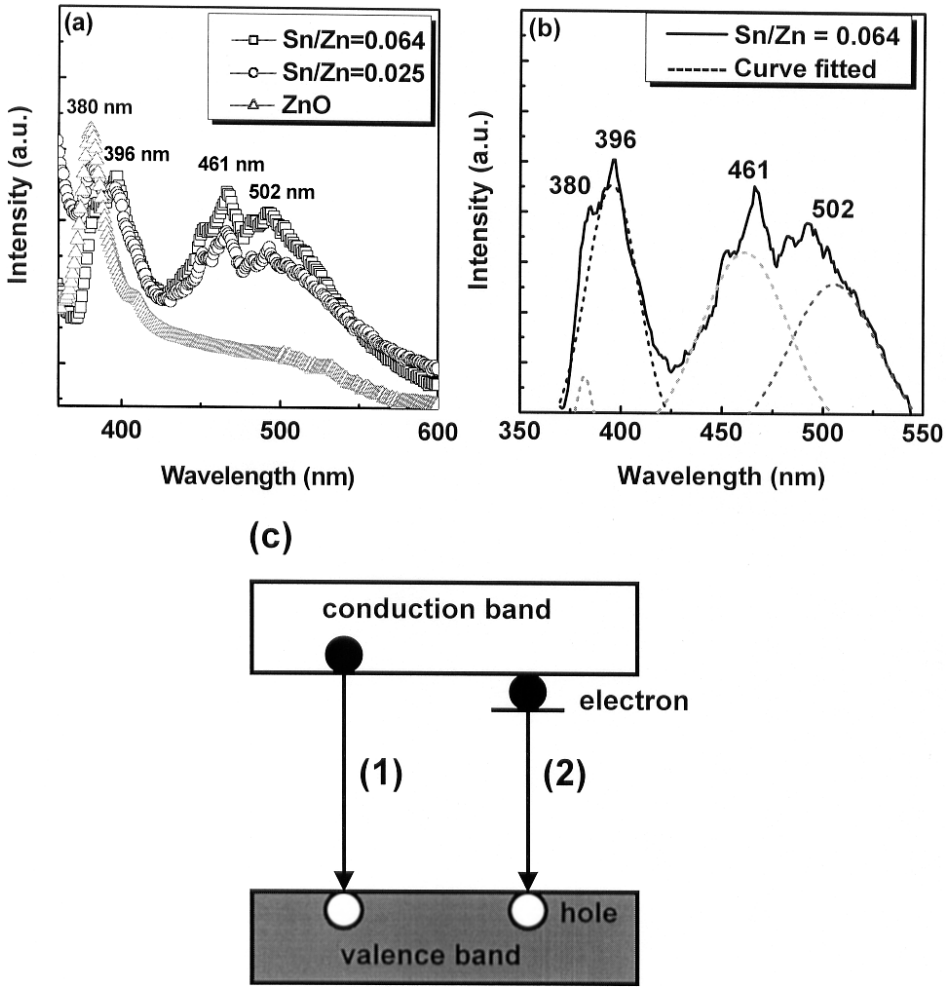

Figure 8. (*a*) PL emission spectra of the updoped and SZO nanowires; (*b*) PL emission curve fitted analysis for 0.3 SZO nanowires; (*c*) proposed energy band structure of the undoped and the SZO nanowires.

396 nm caused by 0.3 SZO nanowires is higher than that of the 0.1 SZO nanowires. There are two other broad PL emissions at $461(E_\lambda = 2.68\,\text{eV})$ and $502(E_\lambda = 2.47\,\text{eV})$ nm in the spectra of the SZO nanowires, which may be associated with complex luminescent centres, such as $(V'_{\text{Zn}} - Sn^{\bullet\bullet}_{\text{Zn}})^{\bullet}$ or Zn_i [22, 23]. Other minor unknown peaks in figure 8 possibly result from the phonon or photon emission processes associated with the thermal atomic vibration in the nanowires.

The field emission characteristics of the undoped ZnO and SZO nanowires are shown in figure 9(*a*). At a current density of $0.5\,\text{mA}\,\text{cm}^{-2}$, the turn-on electric fields of undoped, 0.1 and 0.3 SZO nanowires are $0.83\,\text{V}\,\mu\text{m}^{-1}$, $0.07\,\text{V}\,\mu\text{m}^{-1}$, and $0.05\,\text{V}\,\mu\text{m}^{-1}$, respectively. While the electric field remains at $0.05\,\text{V}\,\mu\text{m}^{-1}$, the electron number densities from the field emission mechanism of the ZnO nanowires are 2.97×10^{15} for 0.3 SZO, 9.93×10^{14} for 0.1 SZO, and 3.77×10^{14} for undoped ZnO nanowires. The released electrons may be increased due to the increase in electric field, and Sn dopant as proposed in equation (1). The lower turn-on electric field and higher electron number density again provide evidence of the substitution of Zn by Sn in the SZO nanowires. The SZO nanowires exhibit better field emission properties than the undoped ZnO nanowires. After the I–V measurement, the Fowler–Nordheim (F–N) relation ($\ln(I^2/E)$ is plotted as a function of $1/E$) is applied in order to realize the properties of those emitters. The F–N plots (indicated in figures 9(*b*)–(*d*)) of those nanowires indicate that the field emission properties of those nanowires follow the F–N equation [24]:

$$J = \frac{A\beta^2E^2}{\phi}\exp\left(\frac{-B\phi^{3/2}}{\beta E}\right), \tag{3}$$

where J is the current density, E the applied field, ϕ the work function of the emitter, β the field enhancement factor, $A = 1.56 \times 10^{-10}$ $(AV^{-2}\,\text{eV})$ and $B = 6.83 \times 10^3$ $(VeV^{-3/2}\,\text{V}\,\mu\text{m}^{-1})$. Therefore, the field enhancement factor and work function can be obtained, respectively, from the slope and the intercept of the F–N plot. The work functions Φ of undoped, 0.1, and 0.3 SZO nanowires are 7.26 eV, 7.16 eV, and 6.92 eV, respectively, while the field enhancement factor, β, of those nanowires are 2.07×10^4, 4.45×10^5, and 6.67×10^5, respectively. The better experimental results are obtained for 0.3 SZO nanowires: $\beta = 6.67\times10^5$ and $\Phi = 6.92$ eV. The field enhancement factors increase and the work function decreases due to the addition of Sn. The larger field enhancement factor is attributed to the smaller diameter of the SZO nanowires. Moreover, it can be concluded from the result that the Sn dopant

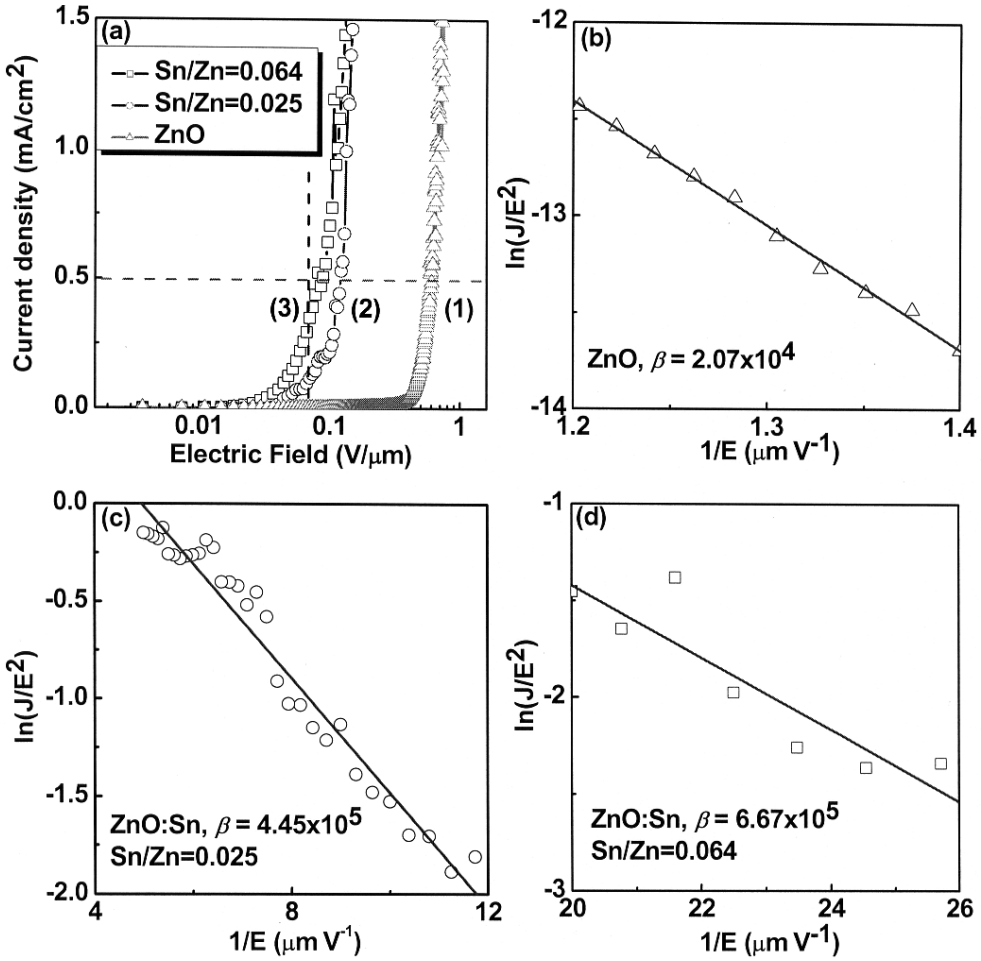

Figure 9. (*a*) Field emission characteristics of the ZnO, (*b*) F–N plots of undoped ZnO, (*c*) F–N plots of 0.1 Sn doped, and (*d*) F–N plots of 0.3 SZO nanowires.

acts as the donor, and this increases the carrier concentration and reduces the work function of the SZO nanowires.

To investigate the difference in electronic characteristics between undoped and SZO nanowires, the stability of the field emission I–V characteristic is compared, as shown in figure 10. The saturation behaviour has been observed on individual undoped, and 0.1 and 0.3 doped ZnO nanowires. The saturation of the field emission current has occurred in those nanowires; that is, each ZnO nanowire has its highest resistance under the turn-on electric field [25, 26]. In this case, the voltage drop (IR) across such a resistor would lead to a decrease in the effective applied voltage, and therefore cause a flattening of the characteristics. The resistance in series with the ZnO nanowires can be estimated by using

$$I = a(V - IR)^2 \exp\left[-\frac{b}{V - IR}\right], \tag{4}$$

where I and V are the field emission current and applied voltage, respectively, a b are constant, and R is the resistance in series with the ZnO nanowires. First, assuming $R = 0$, a, and b can be evaluated by equation (4) fitting to the low emission current part of the measured data. The resistances corresponding to undoped, 0.1 and 0.3 SZO nanowires are estimated to be 85.43 kΩ, 24.53 kΩ, and 8.53 kΩ, respectively, as shown in figure 10. This decrease in resistance is proportional to the increase in Sn dopant concentration. The lower resistance of SZO nanowires is also attributed to the Sn-enhanced electron density and the consequent increase in the conductivity of the ZnO nanowires.

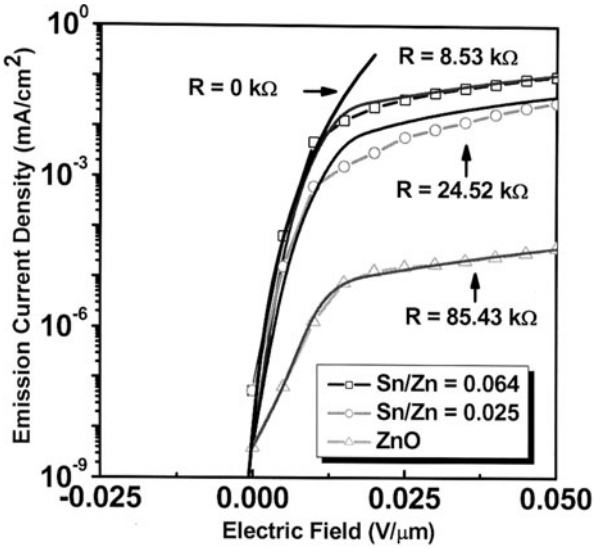

Figure 10. Emission current density versus electric field of the undoped, 0.1, and 0.3 SZO nanowires.

4. Conclusions

In summary, the single crystalline SZO nanowires are fabricated at 800°C under the conditions of a VLS growth process. The morphologies of SZO nanowires are quite different from that of undoped ZnO nanowires due to the occupancy of the Sn atom at the Zn site. This Sn addition also affects the UV emission of SZO nanowires. Furthermore, the 0.3 SZO nanowires exhibit good field emission characteristics of 0.05 V μm^{-1} as the turn-on electric field and 0.5 mA cm^{-2} as the current density. The lower work function of the SZO nanowires is due to the higher carrier concentration and the smaller diameters, which result in the higher field enhancement factor. Therefore, the SZO nanowires could be used for fabricating optoelectronic and field emission devices.

Acknowledgment

The authors acknowledge support by the National Science Council of ROC under contract number NSC 92-2216-E-009-022.

References

[1] Li S Y, Lee C Y and Tseng T Y 2003 *J. Cryst. Growth* **247** 357
[2] Zhang J and Zhang L 2002 *Chem. Phys. Lett.* **363** 293
[3] Wang N, Zhang Y F, Tang Y H, Lee C S and Lee S T 1998 *Phys. Rev.* B **58** 16024
[4] Huang M H, Mao S, Feick H, Yan H, Wu Y, Kind H, Weber E, Russo R and Yang P 2000 *Science* **1292** 1897
[5] Björk M T, Ohlsson B J, Sass T, Persson A I, Thelander C, Magnusson M H, Deppert K, Wallenberg L R and Samuelson L 2002 *Appl. Phys. Lett.* **80** 1058
[6] Bagnall D M, Chen Y F, Zhu Z, Yao T, Koyama S, Shen M Y and Goto T 1997 *Appl. Phys. Lett.* **70** 2230
[7] Lee Y S and Tseng T Y 1998 *J. Mater. Sci. Mater. Electron.* **9** 65
[8] Wang Y W, Zhang L D, Wang G Z, Peng X S, Chu Z Q and Liang C H 2002 *J. Cryst. Growth* **234** 171
[9] Wang R P, Xu G and Jin P 2004 *Phys. Rev.* B **69** 113303
[10] Gomi M, Oohira N, Ozaki K and Koyano M 2003 *Japan. J. Appl. Phys.* **42** 481
[11] Sun H D, Makino T, Tuan N T, Segawa Y, Kawasaki M, Ohtomo A, Tamura K and Koinuma H 2001 *Appl. Phys. Lett.* **78** 2464
[12] Decremps F, Porres J P, Saitta A M, Chervin J C and Polian A 2002 *Phys. Rev.* B. **65** 92101
[13] Li S Y, Lin P, Lee C Y and Tseng T Y 2004 *J. Appl. Phys.* **95** 3711
[14] Li S Y, Lin P, Lee C Y and Tseng T Y *J. Mater. Sci. Mater. Electron.* **15** 505
[15] Morales A M and Leiber C M 1998 *Science* **279** 208
[16] Wu Y, Fan R and Yang P 2002 *Int. J. Nano* **1** 1
[17] Li Y, Meng G W, Zhang L D and Phillip F 2000 *Appl. Phys. Lett.* **76** 2011
[18] Choy J H, Jang E S, Won J H, Chung J H, Jang D J and Kim Y W 2004 *Appl. Phys. Lett.* **84** 287
[19] JCPDS–ICDD 1998 version. 2.0
[20] Chevalier P Y 1988 *Thermo Chem. Acta* **130** 1
[21] Maroie S, Haemers G and Verbist J J 1984 *Appl. Surf. Sci.* **17** 463
[22] Bougrine A, Hichou A E, Addou M, Ebothé J, Kachouane A and Troyon M 2003 *Mater. Chem. Phys.* **80** 438
[23] Hao J H and Cocivera M 2002 *J. Appl. Phys. D: Appl. Phys.* **35** 433
[24] Lee C J, Lee T J, Lyu S C, Zhang Y, Ruh H and Lee H J 2002 *Appl. Phys. Lett.* **81** 3648
[25] Jo S H, Tu Y, Huang Z P, Carnahan D L, Huang J Y, Wang D Z and Ren Z F 2004 *Appl. Phys. Lett.* **84** 413
[26] Bonard J M, Klinke C, Dean K A and Coll B F 2003 *Phys. Rev.* B **67** 115406